Needle Path Control During Insertion in Soft Tissue Using a Force-Sensor-Based Deflection Estimator

Thomas Lehmann[1], Carlos Rossa[1], Ronald Sloboda[2], Nawaid Usmani[2] and Mahdi Tavakoli[1]

Abstract— Needle insertion is commonly used in procedures such as prostate brachytherapy or biopsy. In prostate brachytherapy, the success of the procedure depends on the accurate placement of needles in their pre-planned target location. In order to steer the needle towards a defined target, past research has used ultrasound-image-based needle localization for needle tip position feedback. Acquiring and processing of ultrasound images, however, significantly limits the control sampling rate. This work proposes a method for needle path prediction and control without the need for image feedback. The needle tip path obtained during insertion from a force-sensor-based deflection estimator is used to parameterize a kinematic bicycle model. The bicycle model is then used to predict the needle tip path and the ideal rotation depth for reaching a desired target. Experimental results show that the introduced method accurately predicts the needle tip path and the ideal rotation depth to guide the needle to a pre-defined target.

I. INTRODUCTION

Needle insertion is used in multiple medical fields for drug delivery, biopsy and therapy. In prostate brachytherapy, radioactive seeds are inserted into the prostate with a hollow needle. The needle needs to remain on a straight trajectory during insertion in order to achieve optimal distribution of the radioactive seeds. The beveled tip of the needle, however, causes the needle to deflect from the desired straight trajectory. This is due to the asymmetric geometry of the beveled needle tip, which causes a lateral force to act on it leading the needle tip to follow a curved trajectory during insertion in tissue. The curved trajectory results in a seed placement error and inefficient radiation dosages.

The goal for needle steering in prostate brachytherapy is therefore to steer the needle such that it remains on a straight trajectory. A common method for steering the needle in a two-dimensional plane is rotating the needle by 180° about its longitudinal axis, which reverses the needle tip's trajectory. Using the bevel to steer the needle has been the focus of previous studies. Abolhassani *et al.* [1] showed that it is possible to minimize the deflection by approximately 90%. Others proposed 2D and 3D open- and closed-loop needle steering approaches that make use of image modalities such as ultrasound (US) for position feedback to steer the needle to a pre-defined target location [2], [3], [4], [5], [6], [7].

[1]Thomas Lehmann, Carlos Rossa and Mahdi Tavakoli (Corresponding Author) are with the Department of Electrical and Computer Engineering, University of Alberta, AB, Canada T6G 2V4. E-mail: {lehmann, rossa, mahdi.tavakoli}@ualberta.ca

[2]Ronald Sloboda and Nawaid Usmani are with the Cross Cancer Institute and the Department of Oncology, University of Alberta, Edmonton, AB, Canada T6G 1Z2. E-mail: {ron.sloboda, nawaid.usmani}@albertahealthservices.ca.

The acquisition and processing of images for the measurement of the needle deflection are computationally expensive processes, which result in a significant limitation of the control feedback's sampling time. In clinical practice, it is also not always feasible or possible to obtain US images of the needle at the required axial location.

In our previous work [8], a needle tip deflection estimator was proposed, which uses force and torque measurements at the needle base as input to estimate needle tip deflection. The deflection estimator consists of an analytic quasi-static model, which establishes the relations between assumed needle-tissue interaction loads, and the measured needle base shear force and bending moment. As the analytic modeling approach is computationally efficient, the sampling rate is 50 times higher than image-based deflection measurement.

Since the needle-tissue interaction loads assumed in both [1] and [8] do not model the needle-tissue interactions after rotation, the bicycle model is applied to predict deflection after rotation. Therefore, we propose in this paper a method for predicting a needle tip path with one axial needle rotation taking advantage of our deflection estimator in combination with a kinematic bicycle model. The path prediction is then used to obtain an ideal rotation depth, that brings the needle tip towards a pre-defined target.

A flowchart depicting the individual steps involved in finding the best needle rotation depth for minimum targeting error is shown in Fig. 1. The needle is first inserted in tissue without any axial needle rotation. The deflection estimator (I) takes as input the recorded force/torque data from this insertion and outputs an estimate of the tip path. Parameter fitting (II) is carried out to fit the parameters of the bicycle model onto the estimated tip path. The identified parameters are then supplied to the bicycle model (III), with which several candidate predicted paths are calculated for different rotation depths. Finally, we find the best rotation depth (IV), which leads to the least targeting error. The involved steps are introduced in the following sections.

The paper is structured as follows. The deflection estimator is first introduced in Section II followed by the kinematic bicycle model and the fitting of the bicycle model parameters onto the estimated needle tip path. The method for predicting the needle tip path including one needle rotation using the kinematic bicycle model with the previously identified parameters is then introduced (Section III). Next, the approach for finding the optimal rotation depth is explained. Finally, results of insertion experiments with one rotation at the determined optimal rotation depth are presented in Section V.
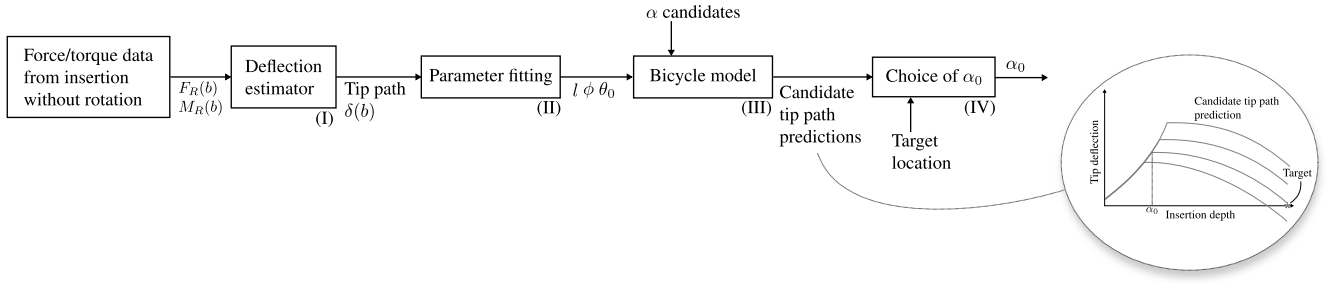
Fig. 1. A flowchart depicting the method for finding the ideal rotation depth α_0. (I) represents the deflection estimator proposed in [8]. It takes as input F_R and M_R, which magnitudes are related to the insertion depth b. The output is the needle tip path, which also depends on b. (II) fits the bicycle model to the estimated tip path obtained from (I), (III) creates candidate paths at different rotation depths α and (IV) chooses the rotation depth, which steers the tip towards the target.
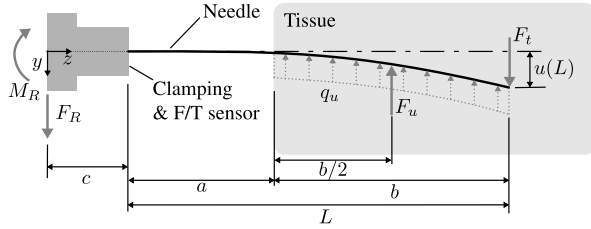

Fig. 2. The model for needle-tissue interactions during needle insertion into tissue [8].

Fig. 3. A schematic representation of the kinematic bicycle model. ϕ is the front wheel's steering angle, l is the length of the bicycle measured from the front wheel's center to the back wheel's center, and r is the radius of the circular trajectory of the bicycle's back wheel. θ is the angle of rotation between the horizontal coordinate and the bicycle. The bicycle's back wheel center is attached to the needle tip.

II. DEFLECTION ESTIMATOR

The first step towards controlling the needle deflection is obtaining an estimate for needle tip deflection. The estimation approach proposed in [8] is used for this purpose. In [8], a quasi-static beam model is devised, which relates the measured forces and moments at the needle base by a force/torque sensor to needle-tissue interaction loads. The needle is modeled as a cantilever beam, which experiences those interaction loads. The needle-tissue interaction model, found in [8] to give an accurate result, corresponds to a uniformly distributed load along the inserted needle portion and a concentrated load at the needle tip. The uniform load q_u represents reaction to tissue compression as the needle shaft deflects during insertion. The concentrated tip load F_t is related to the force applied by tissue at the beveled tip as the tip cuts through tissue [9]. The forces acting on the needle tip during insertion and all needle-tissue interaction loads are depicted schematically in Fig. 2.

The relation between the measured force and moment at the needle base and the interaction loads applied by tissue is established by taking into account the equilibrium conditions, described by [8]:

$$-M_R + F_u(l_1 + c) - F_t(L + c) = 0 \quad (1)$$
$$-F_R + F_u - F_t = 0 \quad (2)$$

with

$$l_1 = a + b\gamma$$

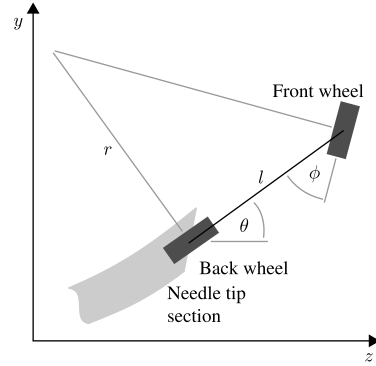where c is the distance between the needle base and the

origin of the force sensor's frame, L is the needle length and γ is the the point at which F_u acts with respect to the proximal tissue boundary. The factor γ therefore takes the value of $1/2$. F_u is the reduction of q_u to a point load and acts at the centroid of q_u. By solving for F_u and F_t, we obtain

$$\begin{bmatrix} F_u \\ F_t \end{bmatrix} = \begin{bmatrix} 1 & -1 \\ l_1 + c & -(L + c) \end{bmatrix}^{-1} \begin{bmatrix} F_R \\ M_R \end{bmatrix}. \quad (3)$$

The deflection model is a static cantilever beam model based on the Euler-Bernoulli beam theory. For a beam experiencing an overall load of $q(z)$, also known as forcing term, along its longitudinal axis z with respect to the needle's base, the deflection $u(z)$ in y direction is governed by a non-homogeneous fourth order differential equation according to Euler-Bernoulli beam theory. As we have two loads acting on the needle (see Fig. 2), in order to obtain the overall tip deflection, the deflections caused by each force are separately calculated and superimposed. The deflections ($\delta_{1,t}$ and $\delta_{2,t}$)
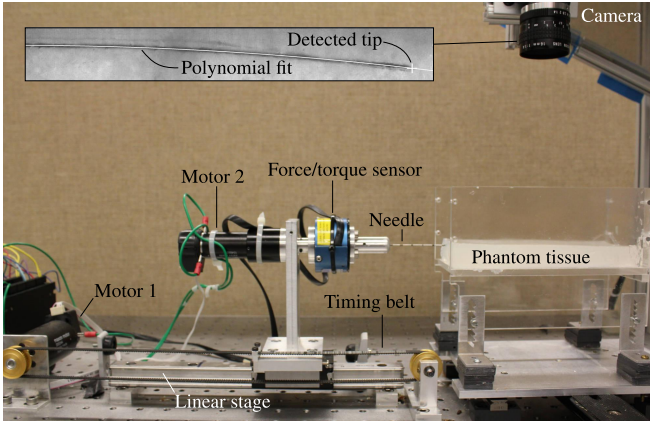
Fig. 4. The experimental setup for performing needle insertions. The two degree-of-freedom robotic system is comprised of a prismatic and a rotational joint. The linear stage, which is actuated by Motor 1 through a timing belt, provides precise linear motion along the needle axis for needle insertion into phantom tissue. Motor 2's shaft holds a force/torque sensor and the needle and rotates the needle about its axis. A camera records images of the needle inside tissue for image-based deflection measurement.

caused by the forces F_u and F_t can be computed as [8]:

$$\delta_{1,t} = \frac{(3L-l_1)l_1^2}{6EI}F_u \tag{4}$$

$$\delta_{2,t} = \frac{L^3}{3EI}F_t \tag{5}$$

The final needle tip deflection is then $\delta = \delta_1 + \delta_2$. The path, which the needle tip takes during insertion $\delta(b)$ can now be constructed through calculating the tip deflection in every discrete step during insertion. The loads shown in Fig. 2 are only valid for needle insertion without axial needle rotation. In order to predict the needle tip deflection after needle rotation, based on measurement obtained from insertion without rotation, we will use the bicycle model, which is described in the following section. The parameterized bicycle model is then used to predict an optimal rotation depth such that the needle tip passes through a desired target location.

III. NEEDLE TIP PATH PREDICTION

The needle tip path beyond the current and up to the final insertion depth needs to be predicted to obtain an optimal rotation depth. Therefore, a kinematic bicycle model is first parameterzed through curve fitting onto the tip path found by the deflection estimator such that a relationship between the bicycle model trajectory and tip path is established. Then, the parameterized bicycle model is again used to predict the tip path including one axial needle rotation.

A. Kinematic Bicycle Model

For finding an optimal rotation depth such that the needle tip reaches a desired target location, a model for predicting the path, that the needle tip will follow is needed. In related work, commonly a kinematic model of a bicycle is used, which was first introduced and adapted for the purpose of modeling multi-bend needle tip path trajectories by Park *et al.* [10] and Webster *et al.* [11]. Since then, the kinematic

bicycle model has become the most commonly used method for needle path planning.

A schematic of the bicycle model is shown in Fig. 3. The kinematic equation for a bicycle model in Euclidean space is [12]

$$\begin{bmatrix} \dot{z} \\ \dot{y} \\ \dot{\theta} \\ \dot{\phi} \end{bmatrix} = \begin{bmatrix} \cos\theta \\ \sin\theta \\ \tan\phi/l \\ 0 \end{bmatrix} v + \begin{bmatrix} 0 \\ 0 \\ 0 \\ 1 \end{bmatrix} \omega \tag{6}$$

where v is the bicycle's translational velocity and hence the needle insertion velocity, ϕ is the front wheel's steering angle and ω is the angular velocity of the front wheel's steering angle and therefore $\dot{\phi} = \omega$. θ is the angle between the horizontal axis and the bicycle. z is the horizontal and y the vertical position of the bicycle back wheel and thus the position of the needle tip. To relate the needle tip path to the bicycle model's planar trajectory, the centre of the rear wheel is attached to the needle tip. To model the needle rotation about $180°$, the sign of the bicycle's front wheel angle ϕ is inverted. Furthermore, at the rotation depth, the bicycle angle θ is set to zero, which sets the bicycle parallel to the horizontal axis. This causes the bicycle model to account for the instant change in direction of the needle tip path at the rotation depth.

B. Parameter Fitting

Now, we need to identify the parameters ϕ, l and θ_0 as shown in Fig. 1, step (III) with a needle tip path estimate obtained from the deflection estimator. θ_0 is the initial angle θ when insertion starts. Insertion data without needle rotation is considered for parameter identification. As (6) contains nonlinearities, the MATLAB® function `lsqcurvefit`, which implements a nonlinear least squares solver, is used. The results of the parameter identification for two different phantom tissue samples are presented in Section V.

C. Optimal Rotation Depth

Once we have identified the model parameters, the bicycle model is used with the previously identified parameters for the particular phantom tissue sample to find the rotation depth α at which the needle needs to be rotated such that the needle tip reaches a desired target at the final insertion depth. Furthermore, after the point of rotation, θ is re-set to zero. Preliminary experiments showed that this results in the best path prediction after rotation.

Multiple different candidate tip paths are constructed using the bicycle model with one rotation at different depths. The final position of the needle tip is different for each candidate path. The optimal rotation depth is now chosen by finding the candidate path, which shows the smallest absolute distance between desired and actual tip location at the final insertion depth.

To verify the accuracy of the chosen optimal rotation depth, insertions in phantom tissue are carried out with one axial needle rotation by $180°$ at the optimal rotation depth. The good match between measured and predicted tip paths shows the successful performance of the path prediction.

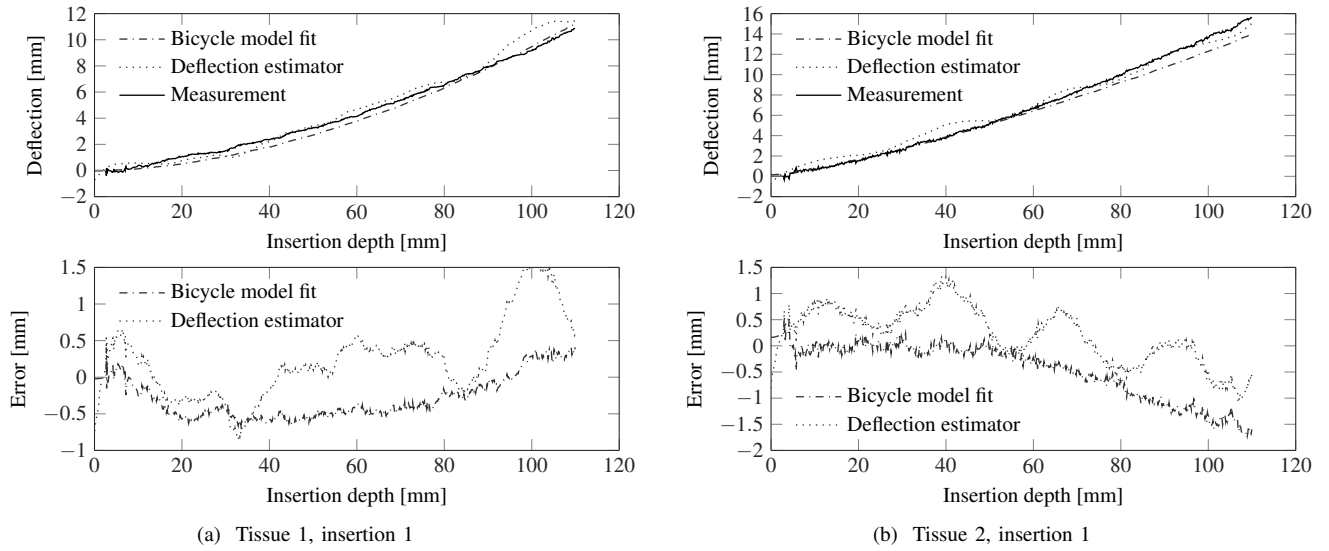(a) Tissue 1, insertion 1   (b) Tissue 2, insertion 1

Fig. 5. The bicycle model fit to the estimated tip path (top plots). The bottom plots show the error between bicycle model trajectory and measured tip path, and the error between deflection estimator and measured tip path.

IV. ROBOTIC SYSTEM FOR NEEDLE INSERTION

The robotic system used to carry out insertion experiments is the 2 degree-of-freedom (DOF) prismatic-revolute system shown in Fig. 4. The needle, which represents the end-effector of the robot, can be translated along (Motor 1) and rotated about (Motor 2) its longitudinal axis. The translational motion is guided by a linear stage. The linear stage's carriage is coupled to a timing belt, which is driven by a DC motor (RE40, Maxon Motor AG, Sachseln, Switzerland). The rotational motor's shaft (RE25, Maxon Motor AG, Sachseln, Switzerland) carries a 6 DOF force/torque transducer (50M31A3-I25, JR3 Inc., Woodland, CA, USA) to record the two corresponding forces and torques, which are the inputs to our model in (3) for needle tip deflection estimation. The sensor's remaining 4 DOFs are not used. Constant velocity insertions are facilitated using a PID controller. For real-time control and data acquisition, Simulink Real-Time™ (MathWorks®, Inc., Natick, MA, USA) is used. The complete system, including a camera for needle deflection measurement and the tissue container, is mounted onto an optical breadboard in order to ensure experiment repeatability.

A. Image-based Needle Deflection Measurement

The needle tip deflection and needle shape during insertion into tissue are measured for experimental validation of the proposed path prediction method. A SONY XCD-SX90CR camera (Sony Corporation, Tokyo, Japan) records images of the needle inside tissue during insertion. The plane of needle deflection is kept parallel to the camera's image plane since only one camera is used to record the needle.

In the sequence of image manipulations, first, the needle contour is extracted from the background. The fact that no needle is present in the initial frame is exploited to remove the background from a frame with needle by subtracting the initial frame from the current frame. A threshold is applied to the differential image to obtain a binary image of the needle contour. The binary image is then converted to a point cloud and a polynomial is fit to the points by using a least-squares approach. To find the needle tip, a window of a pre-defined length is moved along the polynomial fit in the binary image. The tip is detected when the window's sum falls below a pre-defined threshold, meaning that the needle's distal end has been reached. The pixel to mm accuracy is 0.1667 mm/pixel. Sub-pixel accuracy for the measured needle tip location is, however, achieved with the polynomial fit.

V. EXPERIMENTAL RESULTS

In order to collect data for the identification of the bicycle parameters and for the validation of deflection estimates, insertion experiments are performed into two phantom tissue samples made from agar of type *A360-500* (Fisher Scientific International Inc., Hampton, NH, USA). The agar to water ratio for Tissue 1 is 8.3 grams per litre (g/l) and for Tissue 2 is 13.33 g/l. The used needle type is a standard 18-gauge prostate seeding needle of length 200 mm (Eckert & Ziegler BEBIG, Inc. Oxford, CT, USA). The material of the needle is stainless steel, which has a Young's modulus E of 200 GPa. The needle's area moment of inertia I is 7.86×10^{-14} m^4. The needle's bevel angle is 20°.

Two types of insertion are carried out in each tissue sample: one without needle rotation and one with needle rotation by 180° at the optimal rotation depth calculated by the proposed method. The velocity of all insertions is kept constant at 5 mm/s. Six insertions are carried out without rotation to a final depth of 107 mm and three insertions are carried out with rotation at the optimal rotation depth to a final depth of 160 mm.
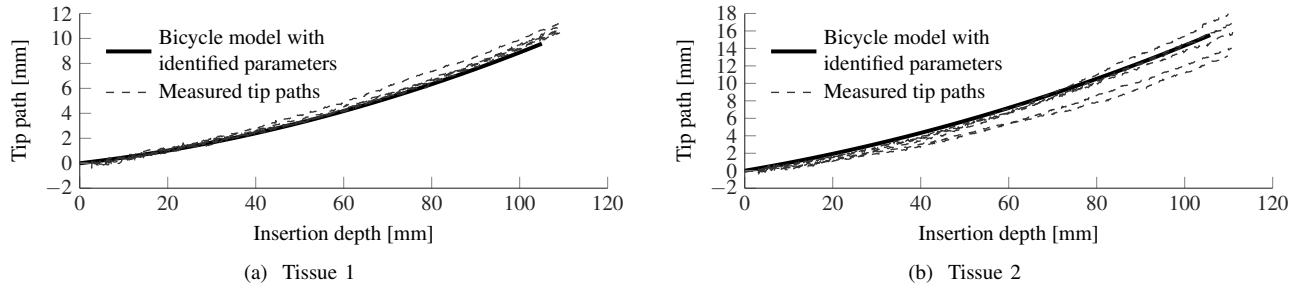
(a) Tissue 1

(b) Tissue 2

Fig. 6. Measured tip paths of six insertions for each tissue and the bicycle model trajectory obtained from the parameter fit.

Tissue #	l [mm]		ϕ [rad]		θ_0 [rad]		α_0 [mm]
	Mean	σ	Mean	σ	Mean	σ	
1	33.33	11.94	0.03	0.003	0.04	0.02	63
2	27.36	7.37	0.03	0.009	0.09	0.02	55

Tissue	Run	Before rotation		After rotation		Accuracy [mm]
		MAE	σ	MAE	σ	
1	1	0.38	0.18	0.63	0.6	-1.05
	2	0.18	0.11	0.40	0.47	-1.30
	3	0.32	0.12	1.13	0.55	-2.26
2	1	0.69	0.31	0.69	0.16	0.6
	2	1.01	0.36	1.01	0.17	1.33
	3	0.84	0.37	0.73	0.2	0.57

The estimated needle tip path using the force/torque sensor approach, along with the measured needle tip deflection in camera images, and the bicycle model fit to the estimated tip path are shown in the top panel of Fig. 5. The estimated tip path via the force/torque sensor is smoothed with a Savitzky-Golay filter prior to parameter fitting. The maximum error between the bicycle model trajectory and the measured tip path is 1.5 mm. The results of the bicycle parameter identification are shown in Table I along with the resulting estimate for the optimal rotation depth α_0. Fig. 6 shows the measured tip paths for six insertions and both tissue samples, and the bicycle model trajectory resulting from the parameters listed in Table I. The fact that the bicycle trajectory is in close proximity to the measured tip paths further demonstrates the quality of the parameter estimate.

To find α_0, i.e. 63 mm and 53 mm, the mean values for ϕ, l and θ_0 presented in Table I are used. The needle is then re-inserted in tissue and rotated at the found rotation depths to validate the prediction performance. Results are shown in Fig. 7. The error between measured and predicted path does not exceed 1 mm throughout insertion. Table II gives a statistical evaluation of the tip path prediction performance with insertions including one axial rotation. The mean absolute error (MAE) is separately evaluated for the path before and after the depth of rotation in order to show that the needle tip path after rotation can be approximated with the identified bicycle parameters with a satisfying accuracy. The maximum MAE for Tissue 1 before rotation is 0.38. After rotation, the maximum MAE increases to 1.13. For Tissue 2, the maximum MAE is 1.01 before rotation and 1.01 after rotation. The targeting accuracy is better for Tissue 2 as only Run 2 shows a higher error than 1 mm where as all insertion runs for Tissue 1 show an accuracy slightly lower than 1 mm. Overall, the absolute average error is 1.54 mm for Tissue 1 and 0.83 for Tissue 2 and the overall absolute average error across both tissue samples is 1.19 mm.

VI. DISCUSSION

It is stated in Section V that insertions up to a depth of only 107 mm are considered for parameter identification. This is due to a loss of the defection estimator's accuracy beyond an insertion depth of approximately 110 mm. The experimental results, however, show that the limited insertion depth consideration for parameter identification is not an issue as it is still possible to obtain a parameter fit with adequate accuracy. Furthermore, the standard deviation σ in Table I for parameter l is fairly high. This is likely due to a variation in the tip path among insertions as Fig. 6 shows. Another likely reason is the noise in the force/torque sensor's signal causing variation in the deflection estimate. Moreover, in Table II, the standard deviations after rotation for Tissue 1, Run 1 and 2 are high. As can be seen in Fig. 7b, a fairly constant offset between predicted and measured tip path exists, which is the cause for the high standard deviation relative to the MAE.

It is shown in Section V that the predicted tip path follows the measured tip path closely according to a maximum MAE of 1.13 after the rotation depth across both tissues and insertions. The error occurring in the path before the depth of rotation can be attributed the fact that the deflection

(a) Tissue 1, insertion 1
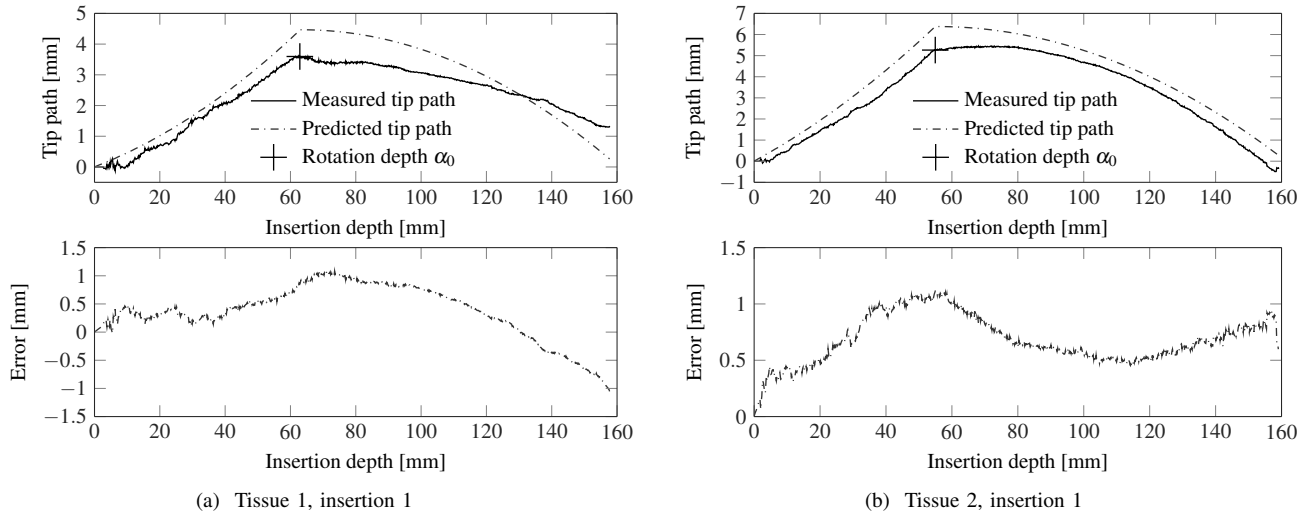
(b) Tissue 2, insertion 1

Fig. 7. The predicted (bicycle model) and measured tip path (top plot) with one rotation, and the error between measured and predicted tip path (bottom plot) for insertions into both tissues.

estimator's tip path estimate contains some remaining imprecision. Furthermore, Fig. 6 shows variation in the measured needle tip paths among insertions. As we do not update the identified bicycle parameters during insertion with axial needle rotation, the model can not adapt to the kind of variations in tip path shown in Fig. 6. The error in the tip path prediction originates from imprecisions in the deflection estimator combined with errors in bicycle parameter fitting caused by noise in the estimated tip path.

VII. CONCLUSION & FUTURE WORK

In this work, a method for needle path control and path prediction is proposed without the need for image feedback. The method consists of a force-sensor-based deflection estimator, which is used to parameterize a kinematic bicycle model for the prediction and control of the needle tip path towards a desired target. It is experimentally validated that the introduced methodology can adequately predict the necessary rotation depth to steer the needle tip towards a pre-defined target and that the target is reached within an absolute average error of 1.19 mm.

Here, the bicycle model is parameterized in an off-line fashion. The parameters are determined from pre-collected experimental data and the found parameters are then assumed constant for future insertions. The needle tip path predicted by the bicycle model can therefore not adapt in case of changing conditions such as changing tissue composition and non-homogeneities encountered during needle insertion. Therefore, our future work will focus on updating the bicycle parameters and the estimation of an optimal rotation depth in real-time during insertion. This will be achieved through a method analogous to the one presented in this paper where the tip path obtained from the deflection estimator during insertion is used for on-line bicycle model parameterization and estimation of optimal rotation depths.

REFERENCES

[1] N. Abolhassani, R. Patel, and F. Ayazi, "Minimization of needle deflection in robot-assisted percutaneous therapy," *The International Journal of Medical Robotics and Computer Assisted Surgery*, vol. 3, no. 2, pp. 140–148, 2007.

[2] S. DiMaio and S. Salcudean, "Needle Steering and Motion Planning in Soft Tissues," *IEEE Transactions on Biomedical Engineering*, vol. 52, no. 6, pp. 965–974, 2005.

[3] K. Reed, A. Majewicz, V. Kallem, R. Alterovitz, K. Goldberg, N. Cowan, and A. Okamura, "Robot-assisted needle steering," *Robotics Automation Magazine, IEEE*, vol. 18, no. 4, pp. 35–46, 2011.

[4] M. Bernardes, B. Adorno, P. Poignet, and G. Borges, "Robot-assisted automatic insertion of steerable needles with closed-loop imaging feedback and intraoperative trajectory replanning," *Mechatronics*, vol. 23, no. 6, pp. 630 – 645, 2013.

[5] M. Abayazid, M. Kemp, and S. Misra, "3d flexible needle steering in soft-tissue phantoms using fiber bragg grating sensors," in *IEEE International Conference on Robotics and Automation (ICRA)*, 2013, pp. 5843–5849.

[6] G. J. Vrooijink, M. Abayazid, S. Patil, R. Alterovitz, and S. Misra, "Needle path planning and steering in a three-dimensional non-static environment using two-dimensional ultrasound images," *The International Journal of Robotics Research*, 2014.

[7] C. Rossa, M. Khadem, R. Sloboda, N. Usmani, and M. Tavakoli, "Adaptive Quasi-Static Modelling of Needle Deflection During Steering in Soft Tissue," *IEEE Robotics and Automation Letters*, vol. 1, no. 2, pp. 916–923, 2016.

[8] T. Lehmann, C. Rossa, N. Usmani, R. Sloboda, and M. Tavakoli, "A Virtual Sensor for Needle Deflection Estimation during Soft-Tissue Needle Insertion," in *IEEE International Conference on Robotics and Automation (ICRA)*, 2015, pp. 1217–1222.

[9] A. M. Okamura, C. Simone, and M. D. O'Leary, "Force Modeling for Needle Insertion Into Soft Tissue." *IEEE Transactions on Bio-Medical Engineering*, vol. 51, no. 10, pp. 1707–1716, 2004.

[10] W. Park, J. S. Kim, Y. Zhou, N. Cowan, A. Okamura, and G. Chirikjian, "Diffusion-Based Motion Planning for a Nonholonomic Flexible Needle Model," 2005, pp. 4600–4605.

[11] R. J. Webster, J. S. Kim, N. J. Cowan, G. S. Chirikjian, and A. M. Okamura, "Nonholonomic modeling of needle steering," *Int. J. Rob. Res.*, vol. 25, no. 5-6, pp. 509–525, 2006.

[12] B. Siciliano, L. Sciavivvo, L. Villani, and G. Oriolo, *Robotics: Modelling, Planning & Control*. Springer, 2011.